

Long Afterglow Green Phosphors Functionalized with Fe-N Doped TiO₂ for the Photocatalytic Removal of Emerging Contaminants

Olga Sacco^a, Vincenzo Vaiano^{a*}, Changseok Han^b, Diana Sannino^a, Dionysios D. Dionysiou^b, Paolo Ciambelli^a

^aDepartment of Industrial Engineering, University of Salerno, Via Giovanni Paolo II 132, 84084 Fisciano (SA), Italy.

^bEnvironmental Engineering and Science Program, Department of Biomedical, Chemical and Environmental Engineering, University of Cincinnati, Cincinnati, OH 10 45221-0012, USA
vvaiano@unisa.it

The aim of this work was to remove oxytetracycline and atrazine using novel catalytic composites consisting of a visible light-active photocatalyst (Fe-N doped TiO₂) supported on visible excited long afterglow aluminate-based phosphors (green phosphors) emitting around 500 nm of wavelength. In the long afterglow Fe-N doped TiO₂/phosphors composites, the light energy (emitted by the lamps used in the tests) is accumulated in phosphors, and then the accumulated light energy emits visible luminescence in dark, which is used as light source for the visible light-active Fe-N doped TiO₂ photocatalysis when the external lamps are turned off.

1. Introduction

Photocatalysis using visible light as energy source is interesting for applications in environmental purification (Vaiano et al., 2014a) as well as solar energy conversion by utilizing visible light of solar and/or indoor light (Zhang et al., 2009). The most used photocatalyst is titanium dioxide (titania, TiO₂) (Vaiano et al., 2014c) that, however, has a wide band-gap of 3.0–3.2 eV (Šíma et al., 2013), allowing to use UV (4-5 % in whole solar spectrum) only, as a consequence, limits its solar applications (Souza et al., 2013).

Metal and non-metal doping has shown encouraging results in extending the light absorption properties of TiO₂ into the visible light region because the band gap of TiO₂ is narrowed by doping. The goal of this work was to develop a visible light-active TiO₂ photocatalyst with iron and nitrogen co-doping (Fe-NT).

In addition to metal and non-metal doping, another way to enhance the photocatalytic activity is the formation of charge transfer complex of TiO₂ and other materials, which can absorb solar light (Wang et al., 2008). It is well known that the interaction of the two different semiconductors (Vaiano et al., 2014b) may cause the charge transfer on the photocatalyst surface to inhibit recombination of photogenerated electron-hole pairs, which improves photocatalytic activity (Li et al., 2012). The long afterglow phosphors such as aluminate-based phosphors (GP) are potential candidates to be combined with Fe-NT (Fe-NT/GP). In the long afterglow Fe-NT/GP composite, the light energy is accumulated in GP, and the accumulated light energy in the GP is emitted as visible luminescence in dark, which can be used as a light source for photocatalysis. In order to investigate the luminescence responsive efficiency of the Fe-NT/GP composite, two different emerging contaminants, the antibiotic oxytetracycline (OTC) and the pesticide atrazine (ATR) are used in photocatalytic process.

2. Experimental

2.1 Catalysts preparation and characterization

The process to obtain Fe-NT/GP was carried out in the absence and in the presence of poly-(ethylene glycol) molecules, i.e. PEG-(200) and PEG-(400), used as binders. Titanium(IV) isopropoxide (TTIP) (>97 % purity,

Sigma Aldrich) was used as a source of titanium dioxide hydrolysed species. A mixture of PEG and TTIP was firstly prepared under stirring at room temperature until an uniform dispersion of PEG was obtained in TTIP. After 48 h of stirring, 5 g of GP was added in the mixture. The GP (provided by DB-Chemic) are excitable by the energy of visible light sources and emit around 500 nm of wavelength. As dopants sources, ammonia aqueous solutions (30% wt.) and iron nitrate with molar ratio N/Ti=18.6 (Sacco et al., 2012) and Fe/Ti=0.44 were used, respectively. The addition of ammonia and iron nitrate was performed at 0 °C under a vigorous stirring, leading to the formation of a precipitate. The precipitate was washed with distilled water and centrifuged several times. Finally, the obtained powders were heated in air up to 450 °C and maintained at this temperature for 30 min. The nominal content of Fe-NT supported on GP surface was 15 wt%. The synthesis procedure is presented in Figure 1. The catalysts were characterized by several techniques. UV–vis reflectance spectra (UV-Vis DRS) of Fe-NT were recorded by a Perkin-Elmer spectrophotometer Lambda 35 using a RSA-PE-20 reflectance spectroscopy accessory (Labsphere Inc., North Sutton, NH). Band gap was determined by plotting $[F(R_{\infty}) \cdot h\nu]^2$ (being $F(R_{\infty})$ the Kubelka-Munk function) vs $h\nu$ (eV). The BET surface area of the samples was measured from dynamic N_2 adsorption measurement at -196 °C, performed by a Costech Sorptometer 1042 after pretreatment at 150 °C for 30 min in He flow. XRD measurements were carried out using an X-ray micro diffractometer Rigaku D-max-RAPID with Cu-K α radiation. The morphology was examined using a scanning electron microscope (SEM, Philips XL 30 ESEM-FEG). In addition, energy dispersive X-ray spectroscopy (EDX) installed in ESEM was employed to observe the Ti, Al, Sr, and Fe distribution on the catalysts surface.

2.2 Photocatalytic tests

ATR and OTC solutions were prepared by dissolving the solid in an appropriate amount of MilliQ-grade water. A Pyrex glass (I.D. =5 cm) petri dish was used as a photoreactor. The glass reactor was sealed with Parafilm and cooled with a fan to prevent evaporation and maintain a constant temperature ($T = 27 \pm 1$ °C). The loading of each photocatalyst in the reaction solution was 0.1 g L^{-1} and the initial concentration of OTC and ATR was 1 mg L^{-1} . The total volume of solution in the photoreactor was 15 mL. The catalysts were maintained in suspension through the use of magnetic stirrer. Two 15 W fluorescent lamps (Cole-Parmer) (Figure 2) were used as a visible light source. For visible light irradiation, a UV block filter (UV420, Opticology) was mounted under the light source and the light intensity was $9.05 \times 10^{-5} \text{ W cm}^{-2}$ determined by a broadband radiant power meter (Newport Corporation). The light sources were fixed at 38 mm from the upper water level in the reactor. The reactor was left under visible light illumination for 3 h for ATR and 2 h for OTC. After, the light sources were turned off and the test solutions were maintained in dark conditions for 3 h for ATR and 1 h for OTC. Throughout the experiments, samples were taken at various time intervals. All the withdrawn samples had a volume of 100 μL and filtered with 0.45 μm pore size filters to remove the catalysts powders. The analyses of OTC and ATR concentrations were performed using an Agilent 1100 Series high performance liquid chromatography (HPLC). The evaluation was carried out using the method described in literature both for ATR (Sacco et al., 2015) and OTC (Zhao et al., 2013).

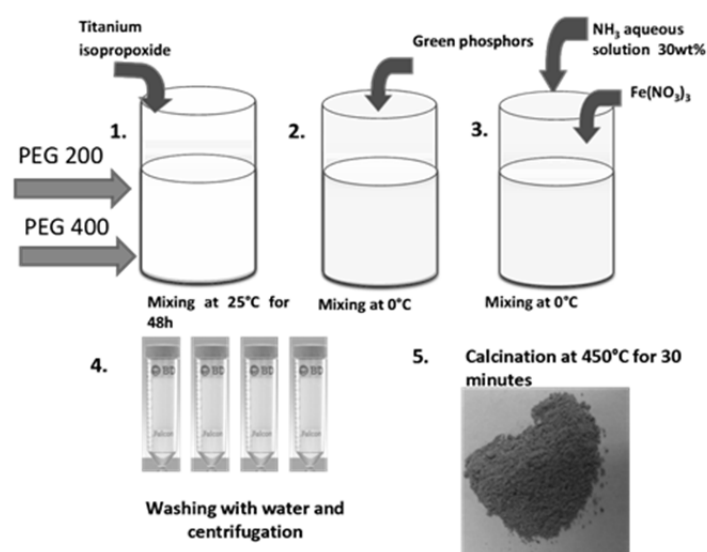


Figure 1 Schematic procedure of the synthesis of Fe-NT/GP composites.

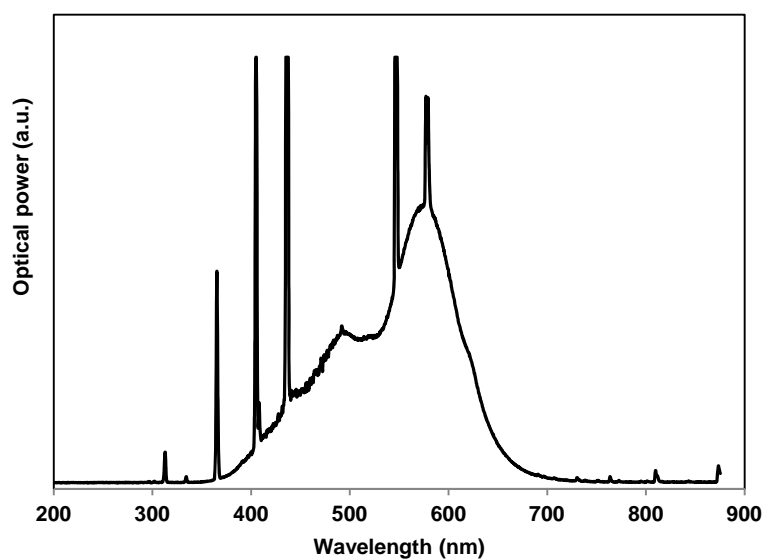


Figure 2 Emission spectrum of light source

3. Results and discussion

3.1 Characterization of the samples

The data obtained from UV-Vis spectra (Figure 3a) showed that Fe-NT catalyst is able to absorb visible light. This data was used for evaluating the band-gap energy (Table 1). As shown in Table 1, the presence of dopants determined a decrease of band-gap value from 3.2 eV, typical of commercial titanium dioxide (Vaiano et al., 2014c) to 2.4 eV. The change in band-gap confirms the ability of Fe-NT to absorb visible light. The crystal phases of Fe-NT and Fe-NT/GP catalysts were determined by XRD analysis (Figure 3b and Figure 4b). For the sample Fe-NT (Figure 3b), all the diffraction peaks can be indexed according to the anatase structure of TiO₂. The XRD spectra of samples 200Fe-NT/GP, 400 Fe-NT/GP (Figure 4b) show the anatase TiO₂ peak at about 25.5°.

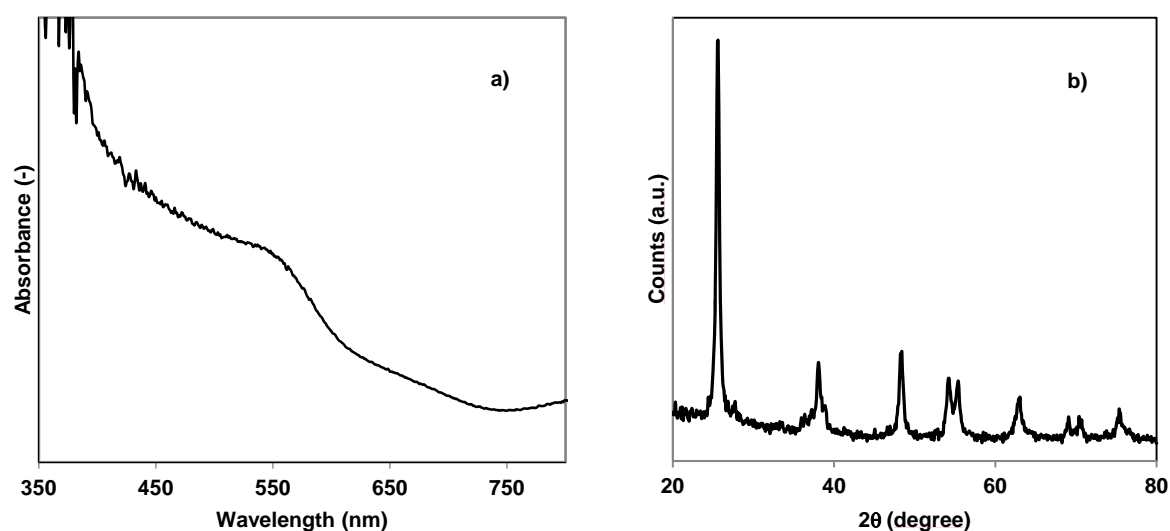


Figure 3 a) UV-Vis and b) XRD spectra of Fe-NT sample.

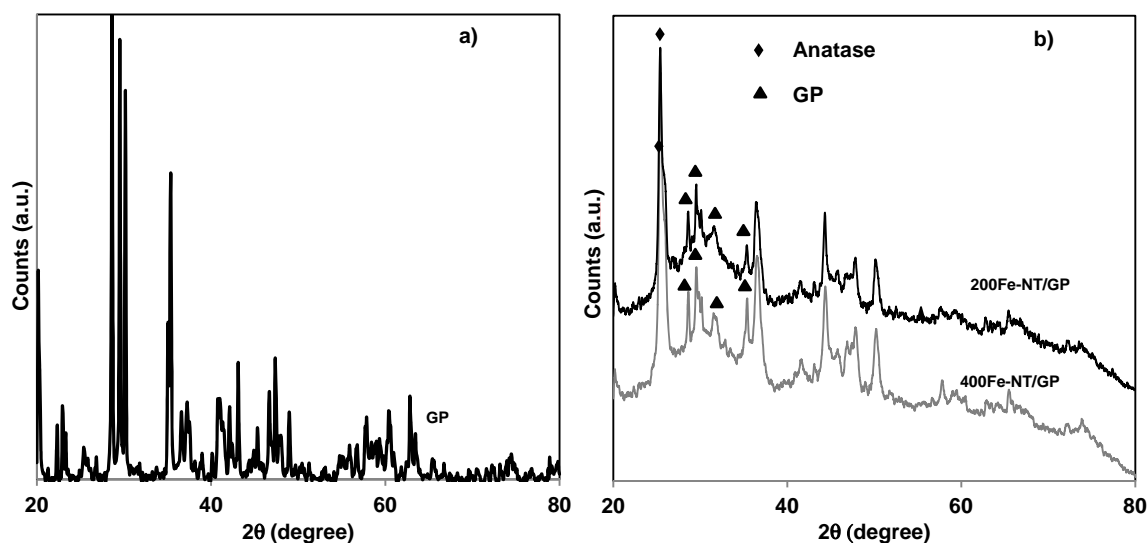


Figure 4 XRD spectra of a) GP and b) Fe-NT/GP samples.

Moreover GP phosphors peaks (28.62° , 28.7° , 29.52° and 35.38°) have not undergone changes of its initial crystallographic structure after deposition of Fe-NT, as it is possible to observe comparing Figure 4a and Figure 4b.

The average size of Fe-NT crystallites was calculated using the Scherrer equation on diffraction plane (1 0 1) for unsupported Fe-NT and supported Fe-NT on GP. The obtained results are reported in Table 1. The Fe-NT average crystallite size was 17 nm. On Fe-NT/GP, the crystallite size of Fe-NT was found smaller and equal to 13 nm when PEG 400 was used, and bigger (22 nm) when PEG 200 was used.

The specific surface areas (SSAs) of all the samples analyzed by BET method are reported in Table 1. The SSAs of Fe-NT catalyst and bare GP samples were very different, being 155 and $0.1 \text{ m}^2 \text{ g}^{-1}$, respectively. It is interesting to note that the SSA of Fe-NT/GP composites increased by increasing the molecular weight of PEG used during the synthesis process. Thus, the addition of PEG allows avoiding a dramatic increase of Fe-NT crystallite size on GP surface, as shown in Table 1.

Figure 5 and Figure 6 show the low-magnification SEM image of GP particles and Fe-NT /GP catalysts, respectively. The morphology of GP (Figure 5a) has irregular shape and the multi-grains agglomerate together forming a cluster. Both composite samples 200Fe-NT/GP and 400Fe-NT/GP show a similar morphology, but with an increased roughness on the surface that is attributed to the deposition of the Fe-NT on the surface. In the same picture (Figure 6), isles of nanoparticles of Fe-NT are visible in some parts. From these observations, it could be concluded that Fe-NT particles were rather uniformly deposited on the surface of micro-sized GP (Figure 6). The atomic composition was analyzed by EDX (Table 1). For GP, it was confirmed that Al and Sr were the prevalent elements with a Al:Sr atomic ratio of 26:72. In the case of 200Fe-NT/GP and 400Fe-NT/GP samples, Ti and Fe are present on the surface of GP as shown in Table 1.

3.2 Photocatalytic activity of Fe-NT/GP catalysts

The photocatalytic activity of Fe-NT and Fe-NT/GP samples for the degradation of ATR was preliminarily investigated for 3 hours under visible light irradiation (Figure 7a).

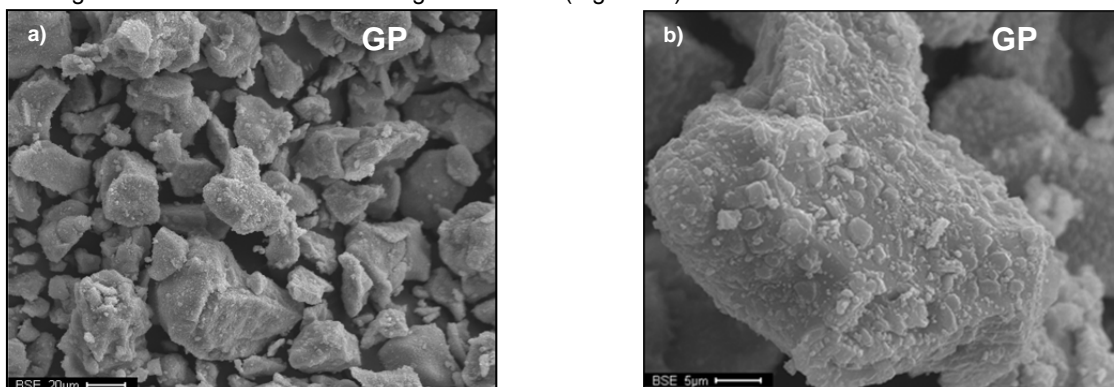


Figure 5 SEM images of GP samples.

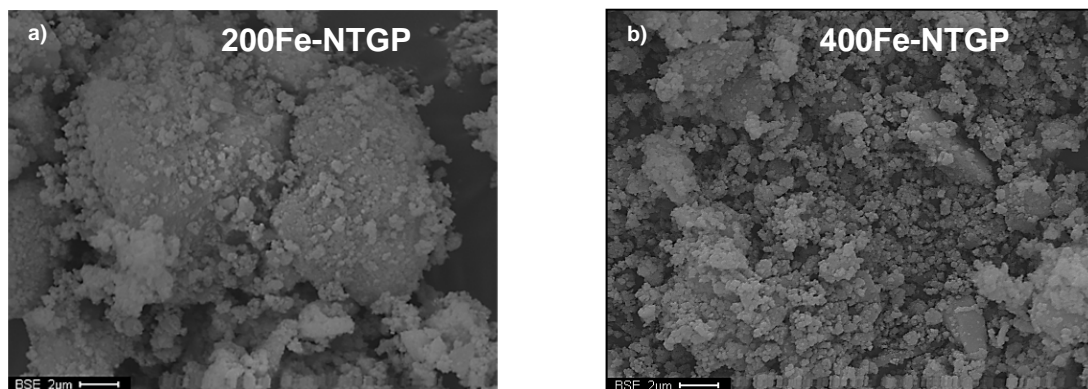


Figure 6 SEM images of 200Fe-NT/GP and 400Fe-NT/GP samples.

After 3 hours of irradiation, the reactor was kept in dark condition for 3 more hours to investigate the effect of GP on the photocatalysis to decompose ATR. The bare GP did not show photocatalytic activity under both visible light irradiation and in dark condition. Fe-NT sample shows photocatalytic activity during the irradiation leading to a degradation of 15 % after 3 h of irradiation and then, when the light was turned off, a little desorption was observed. 200Fe-NT/GP and 400Fe-NT/GP composites show activity both under irradiation and during the dark condition. In particular, the degradation of ATR under irradiation time was equal to 7 % and 3 % and equal to about 22 % in dark condition for 200Fe-NT/GP and 400Fe-NT/GP, respectively. This result can be explained considering that, when the light sources were turned off, the reaction is driven by the light energy accumulated in GP. The accumulated light energy of GP emits visible luminescence, which is used as light source for photocatalysis when the external lamps are turned off. The photocatalytic activity of Fe-NT/GP was also studied in the degradation of OTC (Figure 7b). Also in this case GP did not show photoactivity both under irradiation and in dark conditions. Fe-NT showed photocatalytic activity during the irradiation time, obtaining a degradation of 8% after 120 min of irradiation and it was almost the same when the light sources were turn off. On the other hand, the composite (200Fe-NT/GP and 400Fe-NT/GP) showed photoactivity both under visible light with an OTC removal equal to 9 % and 16 % after 120 min of irradiation and 15 and 21 % in dark condition, for 200Fe-NT/GP and 400Fe-NT/GP, respectively. From the results, it appears that 400Fe-NT/GP photocatalyst showed the highest photoactivity both in ATR and OTC degradation.

4. Conclusions

Visible light-active Fe-N-TiO₂ photocatalyst was successfully immobilized on long afterglow phosphors (GP) by a modified sol-gel method to exploit the photoluminescence of GP. The final nominal loading of Fe-NT on GP surface was 15 wt%. The influence of the addition of PEG in the synthesis process was also studied. The characterization data showed that Fe-NT nanoparticles, dispersed on GP surface, are in anatase phase. With the increase of molecular weight of PEG (from 200 to 400) the crystallites size of Fe-NT dispersed on GP surface, decreased from 22 to 13 nm. This result influenced the photoactivity, which was higher when the Fe-NT crystallites were smaller. This study demonstrates that when supporting a visible light active photocatalysts on afterglow phosphors, the photocatalytic degradation proceeds also after turning off the excitation light.

Table 1: Characterization results of photocatalysts

Catalyst	Crystallites size (nm)	SSA (m ² g ⁻¹)	Eg (eV)	Fe wt%	Ti wt%	Al wt%	Sr Wt%l
GP	-	0.1	-			22.34	62.06
Fe-NT	17	155	2.4			-	-
200Fe-NT/GP	22	18	-	2.1	20.58	16.99	60.32
400Fe-NT/GP	13	30	-	2.87	17.68	19.17	60.13

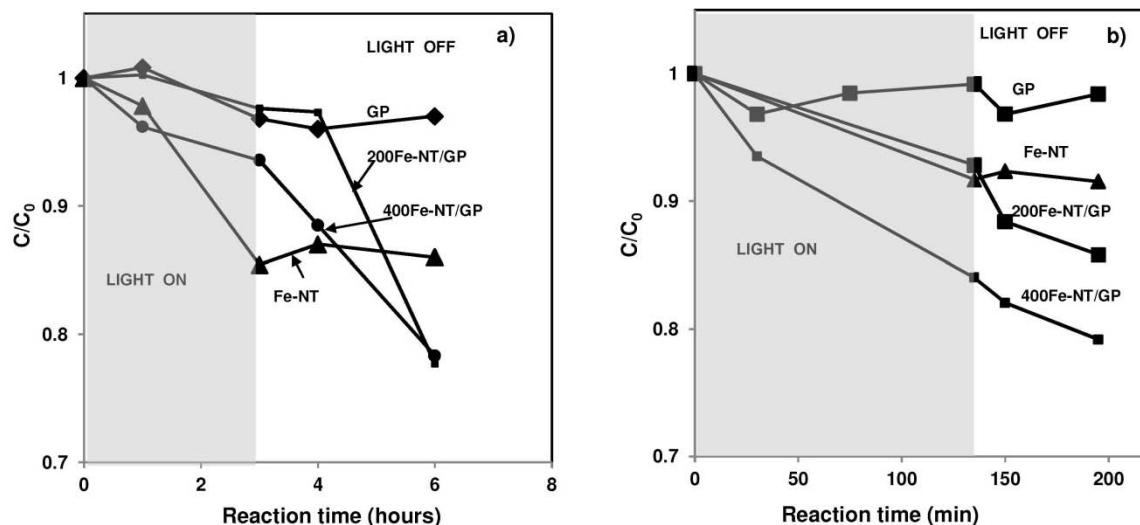


Figure 7 Photocatalytic removal of a) ATR and b) OTC under the visible light irradiation, followed by turning off light (where C/C_0 is the ratio between the concentration at any given time t and initial pollutant concentration).

References

- Li H., Yin S., Wang Y., Sato T. 2012. Persistent luminescence assisted photocatalytic properties of $\text{CaAl}_2\text{O}_4:(\text{Eu},\text{Nd})/\text{TiO}_2-x\text{N}_y$ and $\text{Sr}_4\text{Al}_{14}\text{O}_{25}:(\text{Eu},\text{Dy})/\text{TiO}_2-x\text{N}_y$. *Journal of Molecular Catalysis A: Chemical*, 363-364, 129-133.
- Sacco O., Stoller M., Vaiano V., Ciambelli P., Chianese A., Sannino D. 2012. Photocatalytic degradation of organic dyes under visible light on N-doped TiO_2 photocatalysts. *International Journal of Photoenergy*, Article ID 626759, 8 pages, DOI:10.1155/2012/626759.
- Sacco O., Vaiano V., Han C., Sannino D., Dionysiou D. D. 2015. Photocatalytic removal of atrazine using N-doped TiO_2 supported on phosphors. *Applied Catalysis B: Environmental*, 164, 462-474.
- Šima J., Hasal P., 2013. Photocatalytic degradation of textile dyes in a TiO_2/UV system, *Chemical Engineering Transaction*, 32, 79-84.
- Souza D. A. R., Gusatti M., Sanches C., Moser V.M., Kuhn N. C., Riella H. G., 2013. Initial studies of photocatalytic discoloration of methyl orange by using ZnO nanostructures, *Chemical Engineering Transaction*, 32, 2269-2274.
- Vaiano V., Iervolino G., Sannino D., Rizzo L., Sarno G., Farina A. 2014a. Enhanced photocatalytic oxidation of arsenite to arsenate in water solutions by a new catalyst based on MoO_x supported on TiO_2 . *Applied Catalysis B: Environmental*, 160-161, 247-253.
- Vaiano V., Sacco O., Sannino D., Ciambelli P. 2014b. Increasing the photoactivity of N-doped TiO_2 photocatalysts using phosphors as light carriers. *Chemical Engineering Transactions*, 39, 619-624.
- Vaiano V., Sacco O., Stoller M., Chianese A., Ciambelli P., Sannino D. 2014c. Influence of the photoreactor configuration and of different light sources in the photocatalytic treatment of highly polluted wastewater. *International Journal of Chemical Reactor Engineering*, 12, 1-13.
- Wang J., Li R., Zhang Z., Sun W., Xu R., Xie Y., Xing Z., Zhang X. 2008. Efficient photocatalytic degradation of organic dyes over titanium dioxide coating upconversion luminescence agent under visible and sunlight irradiation. *Applied Catalysis A: General*, 334, 227-233.
- Zhang H., Chen G., Bahnemann D. W. 2009. Photoelectrocatalytic materials for environmental applications. *Journal of Materials Chemistry*, 19, 5089-5121.
- Zhao C., Pelaez M., Duan X., Deng H., O'Shea K., Fatta-Kassinos D., Dionysiou, D. D. 2013. Role of pH on photolytic and photocatalytic degradation of antibiotic oxytetracycline in aqueous solution under visible/solar light: Kinetics and mechanism studies. *Applied Catalysis B: Environmental*, 134-135, 83-92.